Atmos. Chem. Phys. Discuss., 15, 11853–11888, 2015
www.atmos-chem-phys-discuss.net/15/11853/2015/
doi:10.5194/acpd-15-11853-2015


Atmospheric Chemistry and Physics Discussions
Open Access



# Sensitivity of the recent methane budget to LMDz sub-grid scale physical parameterizations

**R. Locatelli, P. Bousquet, M. Saunois, F. Chevallier, and C. Cressot**

Laboratoire des Sciences du Climat et de l'Environnement (LSCE), Gif sur Yvette, France

Received: 25 February 2015 – Accepted: 26 March 2015 – Published: 21 April 2015

Correspondence to: R. Locatelli (robin.locatelli@lsce.ipsl.fr)

Published by Copernicus Publications on behalf of the European Geosciences Union.

## Abstract

With the densification of surface observing networks and the development of remote sensing of greenhouse gases from space, estimations of methane ($CH_4$) sources and sinks by inverse modelling face new challenges. Indeed, the chemical transport model used to link the flux space with the mixing ratio space must be able to represent these different types of constraints for providing consistent flux estimations.

Here we quantify the impact of sub-grid scale physical parameterization errors on the global methane budget inferred by inverse modelling using the same inversion set-up but different physical parameterizations within one chemical-transport model. Two different schemes for vertical diffusion, two others for deep convection, and one additional for thermals in the planetary boundary layer are tested. Different atmospheric methane datasets are used as constraints (surface observations or satellite retrievals).

At the global scale, methane emissions differ, on average, from 4.1 Tg $CH_4$ per year due to the use of different sub-grid scale parameterizations. Inversions using satellite total-column retrieved by GOSAT satellite are less impacted, at the global scale, by errors in physical parameterizations. Focusing on large-scale atmospheric transport, we show that inversions using the deep convection scheme of Emanuel (1991) derive smaller interhemispheric gradient in methane emissions. At regional scale, the use of different sub-grid scale parameterizations induces uncertainties ranging from 1.2 (2.7 %) to 9.4 % (14.2 %) of methane emissions in Africa and Eurasia Boreal respectively when using only surface measurements from the background (extended) surface network. When using only satellite data, we show that the small biases found in inversions using GOSAT-$CH_4$ data and a coarser version of the transport model were actually masking a poor representation of the stratosphere–troposphere gradient in the model. Improving the stratosphere–troposphere gradient reveals a larger bias in GOSAT-$CH_4$ satellite data, which largely amplifies inconsistencies between surface and satellite inversions. A simple bias correction is proposed. The results of this work






ACPD

15, 11853–11888, 2015

provide the level of confidence one can have for recent methane inversions relatively to physical parameterizations included in chemical-transport models.

## 1 Introduction

Inverse modelling techniques are a way to derive sources and sinks of methane using atmospheric measurements as constraints. Today, large uncertainties still affect the recent methane budget estimated by inverse modelling. For example, Kirschke et al. (2013) estimated methane sources between 526 and 569 $Tg\,CH_4\,year^{-1}$ during the 2000–2009 period. The two major causes of uncertainties of methane inversions are the limited and uneven coverage of atmospheric observations and the errors made in the representation of atmospheric transport. However, the increasing number of satellite data retrieving greenhouse gas atmospheric columns and the densification of surface networks in space and time gradually supplement the issue related to atmospheric observations. Consequently, the quality of the representation of atmospheric transport become a major issue in order to improve estimations by inverse modelling. Indeed, inverse modelling requires a model to link methane emissions to methane mixing ratios in the atmosphere. Such a model is generally a chemical transport model (CTM) or a chemistry–climate model (CCM). Then, an atmospheric inversion scheme is applied to greenhouse gas observations to derive the optimal methane source and sink scenario which satisfactory fits both atmospheric observations, given a CTM or CCM, a prior scenario of sources and sinks, and errors for observations, model and emission scenarios (Enting, 2002). The optimal character of such approaches assumes that these errors are properly estimated in magnitude and are unbiased. Indeed, inversions are largely sensitive to any sorts of bias impacting simulated or measured methane mixing ratio. These biases may be related to the CTM and/or the observation datasets, and they directly perturb the optimization of methane fluxes by inverse modelling. Biases in measurements, especially in satellite retrievals, are very likely (Frankenberg et al., 2005; Monteil et al., 2013; Houweling et al., 2014; Bergamaschi et al., 2013).





ACPD
15, 11853–11888, 2015

For example, the first release of SCHIAMACHY data in 2005 were largely biased producing very large tropical emissions (Frankenberg et al., 2005). A major revision has been done to the SCIAMACHY satellite retrievals (Frankenberg et al., 2008) based on a revisit of the spectroscopic parameters for methane, but inversions using SCIAMACHY retrievals still need to carry on large bias corrections up to several tens of ppb (Bergamaschi et al., 2013; Houweling et al., 2014). Systematic errors in CTMs have also significant impacts on inverse estimates. In Locatelli et al. (2013), it was shown that transport model errors are responsible for an uncertainty of 27 Tg $CH_4$ $year^{-1}$ in the estimations of methane fluxes by inverse modelling at the global scale. Moreover, Locatelli et al. (2014) showed that stratosphere/troposphere exchanges are systematically too fast in the version of LMDz (Laboratoire de Météorologie Dynamique model with Zooming capability) using a low vertical resolution (19 levels), which could largely impact the estimation of gas fluxes, like $N_2O$, whose stratospheric mixing ratios influence tropospheric mixing ratios. Besides, following Patra et al. (2011); Locatelli et al. (2013) showed that a bad representation of the interhemispheric exchange in an ensemble of state-of-the-art CTMs can explain most of the discrepancies in the global methane fluxes derived by inverse modelling using these different CTMs.

Inconsistencies in inversions due to CTM errors may have multiple origins: vertical/horizontal resolution, meteorological fields used to nudge horizontal winds, sub-grid scale physical parameterizations, advection schemes, numerical methods, etc. Among the different contributions to CTM errors, the quality of vertical mixing appears to be a key point to improve (Stephens et al., 2007; Geels et al., 2007; Patra et al., 2011). In the vertical, in global models, transport processes such as planetary boundary layer mixing or deep convection have to be parameterized, being on sub-scales of the model grid. Here, we propose to assess the impact of different parameterizations of sub-grid scale transport on the inverted methane emissions for the year 2010. Consequently, we run an ensemble of inversions using different versions of the LMDz model. These LMDz versions differ only by the physical parameterizations they use. Two parameterizations of vertical diffusion (Louis, 1979; Yamada, 1983), one parameterization of





ACPD
15, 11853–11888, 2015

the thermals (Hourdin et al., 2002) and two deep convection schemes (Tiedtke, 1989; Emanuel, 1991) are tested in three different versions of LMDz. As the impact of model parameterizations can be different when either assimilating surface data or satellite column data, we evaluate this impact for three observational systems: two surrface networks and one dataset of GOSAT satellite retrievals.

As a result, this paper is not to be taken as an assessment of the global and regional methane budget for 2010 but more as a study on the sensitivity of this budget to atmospheric transport errors. In the following, Sect. 2 presents the set-up of the ensemble of inversions performed. The consistency between surface-based and satellite-based inversions is then presented and a bias correction is proposed for the satellite data (Sect. 3). The impacts of the different parameterizations used are then analysed through the estimates of methane emissions at the global scale (Sect. 4) and at regional scales (Sect. 5).

## 2 Set-up of variational methane inversions

### 2.1 PYVAR-LMDz-SACS

The PYVAR-LMDz-SACS (Python variational-Laboratoire de Météorologie Dynamique model with Zooming capability-Simplified atmospheric chemistry system) system (Chevallier et al., 2005; Pison et al., 2009) is based on a variational data assimilation system to derive the optimal state of $CH_4$ fluxes given $CH_4$ observations and a background estimate of $CH_4$ fluxes. Variational data assimilation involves minimizing a cost function $J$, which is a measure of both the discrepancies between measurements and simulated mixing ratios and between the background fluxes and the estimated fluxes, weighted by their respective uncertainties, expressed in the covariance matrices **R** (observations) and **B** (prior fluxes), defined as follows:

$$J(\boldsymbol{x}) = (\boldsymbol{y} - \mathbf{H}\boldsymbol{x})^T \mathbf{R}^{-1} (\boldsymbol{y} - \mathbf{H}\boldsymbol{x}) + (\boldsymbol{x} - \boldsymbol{x}^b)^T \mathbf{B}^{-1} (\boldsymbol{x} - \boldsymbol{x}^b) \quad (1)$$



Discussion Paper | Discussion Paper | Discussion Paper | Discussion Paper |

ACPD
15, 11853–11888, 2015

Parameterizations errors in methane inversions

R. Locatelli et al.

*x* is the state vector that contains the variables to be optimized during the inversion process. In PYVAR, methane fluxes are optimized over eight day periods in all the grid cells of the model. The vector $\boldsymbol{x}^b$ represents the prior state of *x*. Likewise, the vector *y* contains the observations of $CH_4$. **B** is the prior error covariance matrix. Its diagonal is filled in with the variances set to 70 % of the square of the maximum of emissions over the nine model grid cells, which contain and surround each grid cell during each month. Off diagonal terms of **B** (covariances) are based on correlation e-folding lengths (500 km over land and 1000 km over sea). No temporal correlations are considered in the **B** matrix. The prior information included in the **B** matrix have several origins:

- $CH_4$ anthropogenic emissions are based on EDGAR v4.2-FT2010 estimates (Olivier and Janssens-Maenhout , 2012),
- $CH_4$ biomass burning emissions are based on GFED3 inventory (Randerson et al., 2013),
- wetland emissions are based on the personal communication of Kaplan (2007) (Bergamaschi et al., 2007).

The **R** matrix accounts for all errors contributing to mismatch between measurements and simulated $CH_4$ mixing ratios. **R** is usually considered as a diagonal matrix because considering covariance dramatically slows down the optimisation and the knowledge about these covariances is too poor. The main contributions to variances are intrumental and model errors. In surface-based inversions, instrumental errors are considered equal to 3 ppb and model errors are computed at each site as the residual SD (RSD) of the measurements on a smooth curve fitting them. The RSD at each site is a proxy of the transport model errors. Previous studies using PYVAR-LMDz-SACS have used this approach (Bousquet et al., 2006; Yver et al., 2011; Locatelli et al., 2013). In satellite-based inversions, GOSAT retrieval random errors are estimated to be about 0.6 % of satellite measurements (Cressot et al., 2014) and a transport model error of 1 % of the observation values is added according to the results of Cressot et al. (2014) on tuning





ACPD
15, 11853–11888, 2015

of error statistics. **H** is the observation operator that projects the state vector $\boldsymbol{x}$ into the observation space. **H** is represented here by the offline version of LMDz complemented by a simplified chemistry module (SACS) to represent the main reactions of the oxidation chain of methane (Pison et al., 2009). The iterative minimizing process implies calculating the gradient of the cost function, which is implemented using the adjoint technique, iteratively solved with the M1QN3 algorithm developed by Gilbert and Lemaréchal (1989) until the gradient norm gets reduced by more than 99 %.

## 2.2 Three different versions of LMDz: LMDz-TD, LMDz-SP and LMDz-NP

LMDz is the general circulation model (GCM) of the IPSL earth system model (Hourdin et al., 2006, 2012b). Here we use an offline version of LMDz implemented in the variational inverse system described in Sect. 2.1. Air mass fluxes are computed and stored using the full GCM and then only the mass balance equation is solved within the variational system, based on the stored air mass fields. In the following, LMDz refers to the offline version of the GCM embedded in the variational system.

In this study, we use three different versions of LMDz using different physical parameterizations (LMDz-TD, LMDz-SP and LMDz-NP) to simulate the atmospheric transport. LMDz-TD uses the physical parameterizations included in the original version of the inverse system of Chevallier et al. (2005): vertical diffusion is parameterized by a local approach from Louis (1979) and deep convection processes are parameterized by Tiedtke (1989) scheme. LMDz-SP uses also a local approach to parameterize vertical diffusion but the Emanuel (1991) scheme parameterizes deep convection. LMDz-NP uses a combination of Yamada (1983) scheme and the thermal plume model of Hourdin et al. (2002) to simulate atmospheric mixing in the boundary layer. Atmospheric transport by deep convection is parameterized by Emanuel (1991).

The horizontal resolution of these three different versions of LMDz is $3.75^{\circ} \times 1.875^{\circ}$ and the vertical discretisation has 39 layers. Some results coming from an old version of LMDz-TD using 19 layers and an horizontal resolution of $3.75^{\circ} \times 2.5^{\circ}$ are also presenteed in Sect. 3.





ACPD
15, 11853–11888, 2015

More details on the characteristics of these three versions of LMDz concerning the modelling of atmospheric transport can be found in Locatelli et al. (2014). Briefly, LMDz-TD is characterized by a low variability in the PBL due to an over-estimation of the PBL mixing. It leads to an under-estimation of the strong gradient observed near sources. On the opposite, LMDz-NP simulates the diurnal cycle of the PBL quite well. The modelling of large-scale atmospheric transport has been also improved with the Emanuel (1991) deep convection scheme. The interhemispheric (IH) exchanges, which are known to be too fast in LMDz-TD version, become more in agreement with the indirectly measured IH exchange when using Emanuel (1991) scheme, as it is done in LMDz-SP and LMDz-NP. However, the Tiedtke (1989) convection scheme is still used in the scientific community, which justify to test it as well in this work.

### 2.3 Three different observation datasets

Different observation datasets exist to constrain methane atmospheric inversions. Surface observations have been assimilated for years, mostly for background or coastal locations. However, more and more continuous and/or continental sites have appeared in the recent years, which largely increase the space and time density of surface observations. Since 2003, satellite data for total methane weighted-columns also exist, largely increasing spatio-temporal coverage of observations but at the cost of a lower precision of individual measurement. In this study, two surface observation datasets (Sect. 2.3.1) and one GOSAT satellite dataset (Sect. 2.3.2) are used to constrain our inversions.

#### 2.3.1 Two surface observation datasets

Two networks of surface stations have been used in the different inversions of this study: the "background" and the "extended" networks. Red circles on the Fig. 1 represent the location of surface stations in the "background" network. The "background" (BG) network is mainly representative of "background" air since most of the surface





ACPD
15, 11853–11888, 2015

stations of this network are located far away from the main methane sources. The "extended" (EXT) network is an extension from the "background" network, where 24 stations are added to the "background" network (blue circles on the Fig. 1). These addtitional stations have been selected for their continental footprint, closer to methane emissions than most of the background sites and therefore providing more direct information on methane emissions. However, being closer to emission areas, and generally located inland, they show more variable mixing ratios and are more sensitive to transport errors (Locatelli et al., 2013). In the following, we use BG and EXT to respectively refer to surface measurements in the background and extended configuration of the surface network.

Inversions using these surface observations datasets have been run between 2006 and 2012, but we mainly present results for 2010 to be consistent with the satellite inversions.

#### 2.3.2 One satellite dataset: GOSAT satellite

Methane total weighted-columns retrieved by GOSAT satellite are also used in our study to constrain methane inversions. Version 4.0 of the TANSO-FTS $XCH_4$ proxy retrievals performed at the University of Leicester (Parker et al., 2011) are used with associated averaging kernels and a priori profiles. In the "proxy" method, it is considered that $CO_2$ and $CH_4$ spectral absorption bands are close enough to assume that light path perturbations affecting $CO_2$ total-column mixing ratio are similar to those affecting $CH_4$ total-column mixing ratio. Thus, the ratio between the measured $CH_4$ and $CO_2$ vertical mixing ratio is not affected by any perturbations due to aerosol scattering and clouds. Consequently, the total column of $CH_4$ ($XCH_4$) is computed according to: $XCH_4 = \frac{[CH_4]_{meas}}{[CO_2]_{meas}} \times XCO_{2mod}$, where $[CH_4]_{meas}$ and $[CO_2]_{meas}$ are respectively the $CH_4$ and $CO_2$ measured mixing ratio, and $XCO_{2mod}$ is a model-derived estimate of $XCO_2$ coming from Chevallier et al. (2010).

In the following this dataset is referred as PR-LEI standing for "Proxy-Leicester".





ACPD
15, 11853–11888, 2015

Data from July 2009 to June 2011 are used in the inverse procedure to extract the inferred methane fluxes for the year 2010 with limited time side effects.

## 3 Consistency between surface-based and satellite-based inversions

Surface observations provide accurate methane mixing ratios but are unevenly distributed in time and space. The use of total column $CH_4$ retrievals from satellite is fundamental for global inversions as it provides constraints within regions not sampled by surface stations. In particular, satellite data give valuable information in tropical regions, which are known to largely contribute to global methane budget and where few surface measurements are available. However, uncertainties may be significant in satellite datasets. For example, Houweling et al. (2014) and Bergamaschi et al. (2013) have shown that SCIAMACHY satellite retrievals were usable in methane inversions only if a bias correction algorithm was added. Monteil (personal communication, 2014) has also shown inconsistencies between surface and GOSAT satellite inversions, which could be explained by space or time dependant biases in GOSAT retrievals. Another reason could be due to discrepancies in the modelling of methane vertical transport in the atmosphere. Here, using the different versions of the LMDz model, we estimate the inconsistencies between surface-based and satellite-based inversions and we investigate the impact of the representation of vertical transport on these inconsistencies.

Four inversions are perfomed using GOSAT data without any bias correction using the three versions of LMDz (LMDz-TD, LMDz-SP, LMDz-NP as described in Sect. 2.2) and the former 19-layer model version (LMDz-19) related to LMDz-TD (Chevallier et al., 2005). The optimized atmosphere is then sampled at surface stations and compared to surface observations for the four different versions of the LMDz model (Fig. 2). Figure 2 shows that methane surface mixing ratios simulated from optimized fluxes using GOSAT satellite retrievals do not fit methane mixing ratios directly measured at surface stations. The different 39-layer versions of the LMDz model show a bias of about +40 ppb, with only a small latitudinal dependency. This means that, at the surface, the





ACPD
15, 11853–11888, 2015

optimized atmospheric methane concentrations seen by GOSAT are 40 ppb higher on average than the observed atmosphere. Such a bias can be due to satellite retrievals and/or transport model errors.

The similarity of biases derived by LMDz-TD, LMDz-SP and LMDz-NP (Fig. 2) highly suggests that sub-grid scale parameterizations of vertical transport only play a minor role on inconsistencies between surface and simulated (based on satellite retrievals constraints) methane mixing ratio. Monteil (personal communication, 2014) found similar results performing different sensitivity tests to explain inconsistencies between surface-based and satellite-based inversions. As a result, we can conclude that parameterizations of deep convection and diffusion are likely not the cause of these inconsistencies.

Interestingly, we find a very different result with the 19-layer version of LMDz (LMDz-19). Indeed, LMDz-19 derives a smaller bias (+15 ppb in the high latitudes of the Southern Hemisphere decreasing to −10 ppb in the Northern Hemisphere). LMDz-19 differs from LMDz-TD only by a coarser vertical resolution. Therefore, a higher vertical resolution seems to degrade the bias of GOSAT inversions, despite the improvement of large-scale transport presented in Locatelli et al. (2014) for this new version of LMDz.

In order to explain this large difference between the two vertical resolutions of the LMDz model, we compare the simulated vertical profiles of methane mixing ratios using LMDz-TD with 19 (LMDz-19) and 39 (LMDz-39) vertical levels (Fig. 3). Both simulated profiles use the corresponding optimized methane fluxes derived by inversions using the same atmospheric constraints (GOSAT PR-LEI). Figure 3 shows that $CH_4$ profile is very sensitive to the vertical resolution. The largest differences are found in the stratosphere: LMDz-19 simulates much higher stratospheric methane mixing ratios compared to LMDz-39. On the contrary, and consistently with mass balance, LMDz-19 tropospheric mixing ratios are smaller than LMDz-39. As found in Locatelli et al. (2014), the two versions of the model have very different abilities to reproduce stratosphere/troposphere exchange (STE). STE is particularly fast in LMDz-19 compared to LMDz-39, which induces stronger methane mixing ratio in the stratosphere in LMDz-19.

One could think that LMDz-19 simulates a more consistent methane vertical distribution than LMDz-39 as biases on Fig. 2 are smaller for LMDz-19 than for LMDz-39. However, we have compared the modelled methane mixing ratio vertical gradients with the climatology from the HALOE instrument (Grooß and Russel III, 2014), and we have found extremely similar gradients between LMDz-39 and HALOE data. Indeed, the methane gradient between 200 and 3 hPa is 2.2, 5.5 and 5.3 ppb $hPa^{-1}$ for respectively LMDz-19, LMDz-39 and HALOE. As a result, we find that the relative contribution of each vertical layer to the total column is very different in LMDz-39 and LMDz-19 (lines with cross markers on Fig. 3). Stratospheric (Tropospheric) layers in LMDz-39 contribute much less (more) than in LMDz-19. Consequently, the inverse system derives lower methane fluxes with LMDz-19 to simulate lower tropospheric methane mixing ratio compensating the over-contribution of stratospheric methane mixing ratio to the total-column.

Thus, the relatively small bias found in the validation of LMDz-19 satellite flux by surface measurements is unfortunately due to an inadequate representation of the troposphere/stratosphere methane mixing ratio gradient. LMDz-39 derives a stronger bias between simulated and surface measurements, but we can assert that this bias is not due to errors in the modelling of troposphere/stratosphere gradient. To conclude, the reasons of such biases in the satellite data still need more attention on the model side, but most probably also on the data side.

In order to analyse methane fluxes despite these inconsistencies, satellite–based inversions are performed in two steps. Firstly, we run inversions using GOSAT data without adding any bias corrections. Secondly, we remove the latitudinal bias found when we compute the difference of the concentrations simulated at each surface stations using the optimized methane fluxe coming from the first inversion with the surface observations considered as unbiased. In the following, in addition to surface-based inversions, we only focus and present results associated to these two-step satellite-based inversions.





ACPD
15, 11853–11888, 2015

## 4 Impact of physical parameterizations on global methane fluxes

Figure 4 displays the sensitivity of the global methane budget to physical parameterizations by showing the global methane estimates from nine inversions using the three different versions of the model (Sect. 2.2) and the three different datasets (Sect. 2.3). Using the BG, EXT, and PR-LEI datasets to constrain methane inversions, we found that the spread (min-max) in derived methane emissions due to changes in physical parameterizations is respectively 2.7, 7.5, and 2.1 Tg $CH_4$ in 2010. It respectively represents 0.5, 1.4 and 0.4 % of methane global emissions. However, these spreads are much lower than the 27 Tg $CH_4$ found in the pseudo-experiment of Locatelli et al. (2013), which was estimated as a "total" transport model errrors. "Total" here refers to all the possible causes of transport errors. The use of different physical parameterizations within the same CTM integrated in the same inverse system has a significant impact on global methane emissions, although smaller than using different CTMs as it is done in Locatelli et al. (2013). Indeed, we only test here few parameterizations of the vertical transport in one model. Transport models can also differ in their horizontal resolution and horizontal advection, in their meteorological forcings and the way they constrain atmospheric transport, and in the coupling between their different characteristics.

The largest spread (7.5 Tg $CH_4$) is found for the EXT inversions. It is especially due to the EXT-NP inversion, which estimates global methane emissions of 539.8 Tg $CH_4$ in 2010 compared to 532.3 and 533.3 Tg $CH_4$ for respectively EXT-TD and EXT-SP. In particular, this large estimation is due to a specific region, China. The impact of the parameterizations on China methane flux estimates is further discussed in Sect. 5.

We find that, at the global scale, the spread in GOSAT satellite inversions (2.1 Tg $CH_4$) is lower than both BG (2.7 Tg $CH_4$) and EXT (7.5 Tg $CH_4$) surface-based inversions. First, sub-grid scale parameterizations in chemistry-transport models mainly impact the modelling of vertical transport. An inaccurate representation of methane vertical distribution has larger impacts on simulated mixing ratios at the sur-





ACPD
15, 11853–11888, 2015

face than on simulated total-column. Indeed, a simulation of surface methane mixing ratios, which takes place at a specific level of the atmosphere, could miss or underestimate a methane plume if, for example, methane is transported too quickly in the upper atmosphere. On the contrary, simulated total-column would not miss this methane plume since it would stay in the atmospheric column, even if the methane plume is simulated at a wrong level. Secondly, surface sources induce weaker signatures in the total column amounts than in surface concentrations (Rayner and O'Brien, 2001), which could result in a smaller sensitivity of the inverse system to total-column than to surface measurements.

Discrepancies in global methane estimates derived by inverse modelling are usually largely explained by large-scale characteristics of the modelling of interhemispheric (IH) exchanges. For example, the overestimation of the north/south gradient in methane mixing ratios in the a priori simulations of the TM5 model have been assumed to be caused by too slow IH exchanges in TM5 (Houweling et al., 1999; Bergamaschi et al., 2009; Monteil et al., 2013). Furthermore, in Patra et al. (2011), LMDz-TD (using a coarser horizontal and vertical resolutions than the version of LMDz-TD used here) is in the range of CTMs simulating a too fast IH exchange, which have been shown to induce a positive (negative) bias in methane emissions in the Northern (Southern) Hemisphere (Locatelli et al., 2013) after inversion.

In order to investigate the representation of IH exchange in our inversions, we present in Table 1 the methane estimates in the Northern and the Southern Hemispheres, and IH methane emission gradient for the common year (2010) of the different inversions. Whatever the constraints used in our inversions, IH gradients simulated by LMDz-TD are larger compared to those simulated by LMDz-SP. Indeed, BG, EXT, and PR inversions using LMDz-TD respectively derive IH gradients 21.2, 31.5 and 1.0 Tg $CH_4$ higher than in inversions using LMDz-SP. These results confirm the conclusion of Locatelli et al. (2014) who have shown that LMDz-SP simulates IH exchange slower than LMDz-TD based on an analysis of $SF_6$ simulations. Indeed, LMDz-SP simulating slower IH exchange finds, on average, higher (smaller) methane mixing ratios





ACPD
15, 11853–11888, 2015

in the Northern (Southern) Hemisphere than in LMDz-TD. In response, the inverse system using LMDz-SP derives smaller (higher) methane emissions in the Northern (Southern) Hemisphere to fit the oberved mixing ratio. This leads to a smaller IH gradient in methane emissions compared to what the inverse system derives when it uses LMDz-TD.

Concerning LMDz-NP, results are slightly different. In surface inversions, IH gradients simulated by LMDz-NP are also smaller than those simulated by LMDz-TD, even if the difference is smaller between LMDz-NP and LMDz-TD than between LMDz-SP and LMDz-TD. However, these results are in agreement with the study of Locatelli et al. (2014), which has shown that the thermal plume model implemented in LMDz-NP was responsible for a faster IH exchange in LMDz-NP than in LMDz-SP. Thus, we are not surprised to simulate an IH gradient of 6.0 (BG inversions) and 25.6 Tg $CH_4$ (EXT inversions) higher in LMDz-NP than in LMDz-SP. Moreover, the larger difference in EXT compared to BG inversions can be explained by the higher number of stations located closer to methane sources, where the thermal plume model strongly affects the boundary layer mixing (Locatelli et al., 2014).

However, the stronger IH gradient simulated by PR-LEI-NP was not expected from the study of Locatelli et al. (2014). Indeed, PR-LEI-NP simulates an IH gradient of 262.0 Tg $CH_4$, which is surprisingly higher than PR-LEI-TD (249.9 Tg $CH_4$). Large methane emissions are derived in tropical regions for the year 2010. These regions are across the equator and experience important vertical mixing during the year (e.g. moonsoon in India). Therefore, they are sensitive to the parameterization of this transport. A small but wrong repartition between Northern and Southern Hemisphere of emissions from these regions can strongly affect the IH gradient computed here. Moreover, satellite inversions generally derive stronger methane emissions in the Tropics than surface-based inversions (Bergamaschi et al., 2013; Monteil et al., 2013; Houweling et al., 2014). For example, Houweling et al. (2014) found a shift in the emissions from the extra-tropics to the tropics of $50 \pm 25$ Tg $CH_4$ year$^{-1}$. Thus, one can expect that IH gradient can be changed in satellite-based inversions because emissions can easily





ACPD
15, 11853–11888, 2015

be attributed to southern or Northern Hemisphere. On the contrary, surface inversions do not have enough constraints to derive accurate tropical emissions which are expected to be high due to strong wetlands and biomass burning methane emissions. The "missing" amount of methane emissions in tropical regions derived by surface inversions are generally shifted to extra-tropics, which lead to less ambiguous definition of the interhemispheric gradient since emissions are clearly attributed to one of the two hemispheres. Moreover, we expect that PR-LEI-NP would simulate a smaller IH gradient for a year without such large emissions in the Tropics (Houweling et al., 2014).

Overall and across the different datasets assimilated, the largest spread in methane global emission estimations due to parameterization errors reach 7.5 unitTg $CH_4$ year$^{-1}$, representing 1 % of the total global of methane emissions. The choice of the deep convection scheme has a significant impact on the relative distribution of methane emissions between extra-tropical and tropical regions because deep convection impact strongly large-scale atmospheric transport. Versions of LMDz using the deep convection of Emanuel (1991), like LMDz-SP and LMDz-NP, produce a smaller interhemispheric gradient in methane emissions, improving one of the PYVAR inverse system's flaws identified in Patra et al. (2011) and Locatelli et al. (2013). Among datasets, the impact of parameterization uncertainties on methane emission estimations is smaller when using satellite total-column data compared to surface observations, suggesting than errors related to the modelling of vertical transport have less impacts on estimations when considering total-column data.

## 5 Impact of physical parameterizations on regional methane flux estimates

Figure 5 gives a representation of methane flux estimations derived by the nine inversions for 12 continental regions in 2010. The black lines represent values of prior methane emission for each region. Estimations using LMDz-TD (LMDz-SP and LMDz-NP) are plotted in shades of red (green and blue respectively). Comparing estimates





ACPD
15, 11853–11888, 2015

derived by the different inversions allows us to analyse the impact of sub-grid scale parameterizations on regional inverted estimates.

In the BG configuration of surface-based inversions (the first three barplots for each region), larger differences are found between inversions using different deep convection schemes than between inversions using different parameterizations of boundary layer mixing. In tropical regions, where deep convection is predominant, like in South America Tropical, South East Asia or India, it is expected that BG-SP and BG-NP, which both use the deep convection scheme of Emanuel (1991), derive similar estimate, while BG-TD, which uses the deep convection scheme of Tiedtke (1989) derive slightly different estimations. For example, BG-SP and BG-NP derive respectively estimates of 79.0 and 79.2 Tg $CH_4$ year$^{-1}$ in South East Asia, compared to 76.5 Tg $CH_4$ year$^{-1}$ for BG-TD. For extra-tropical regions, where deep convection is less predominant, like in North America Temperate, Europe or China, the representation of interhemispheric exchange can have large impacts on regional estimates. Indeed, BG inversions are mainly constrained by remote stations (see Sect. 2.3.1), where simulated concentrations are largely impacted by the representation of large scale transport (like interhemispheric exchange). As mentioned in Sect. 4, the deep convection scheme of Emanuel (1991) has improved the representation of interhemispheric exchange in LMDz. Thus, LMDz-SP and LMDz-SP both using Emanuel (1991) scheme derive similar estimates in regions like North American Temperate, Europe or China. Flux estimations for boreal regions (like North America Boreal and Eurasia Boreal) are also strongly dependent of the modelling of large-scale atmospheric transport since they are far from the main sources of methane. Then, LMDz-SP and LMDz-NP derives also similar estimates in these two boreal regions.

In EXT inversions, the thermal plume model (combined with the Yamada (1983) scheme) implemented in LMDz-NP has large impacts. Indeed, this scheme plays a key role on the mixing in the boundary layer and can produce large differences in methane mixing ratio simulated for stations located close to high methane sources as in the EXT network. Thus, large impacts are found in China (5 stations have been added close to

China in the EXT network) where EXT-NP derives emissions of 74.7 Tg $CH_4$ $year^{-1}$ compared to 68.2 and 67.2 Tg $CH_4$ $year^{-1}$ for respectively EXT-SP and EXT-TD. Tropical regions (like in South America Tropical) are also affected by the thermal plume model, even if the reasons are less obvious than in China. Indeed, there are still very few stations constraining tropical emissions in the EXT network.

On the contrary, in PR-LEI inversions, GOSAT data bring strong constraints in tropical regions where methane sources are supposed to be large. Thus, it is not surprising to see large impacts on tropical region estimates in satellite-based inversions due to the implementation of the thermal plume model, which plays an important role at the base of deep convection layers (Locatelli et al., 2014) (see the last three barplots on Fig. 5). Indeed, PR-LEI-TD and PR-LEI-SP derive methane emissions of 68.3 and 67.0 Tg $CH_4$ $year^{-1}$ in South East Asia, while PR-LEI-NP derives methane emissions of 80.7 Tg $CH_4$ $year^{-1}$ in the same region. In South America, PR-LEI-TD and PR-LEI-SP derive larger methane emissions (68.4 and 67.7 Tg $CH_4$ $year^{-1}$) compared to PR-LEI-NP which derives methane emissions of 62.0 Tg $CH_4$ $year^{-1}$. As a consequence, satellite-based inversions derive very different spatial distribution in methane emissions between the different tropical regions, although their total methane emissions in the Tropics remain close.

More quantitatively, Table 2 summarizes the spread (difference between the maximum and the minimum of methane emission estimations) in BG, EXT and PR-LEI inversions due to changes in physical parameterizations. The spread is expressed in percentage and in Tg $CH_4$ $year^{-1}$. The numbers are relative to the common year of inversions, which is 2010. However, average spreads between 2007 and 2011 are also shown for BG and EXT inversions (inside the brackets in Table 2) since surface-based inversions have been run for several years. First, one can notice that the spreads (in percentage) at regional scales caused by changes in sub-grid scale parameterizations appear larger compared to what was found at the global scale (see Sect. 4). Indeed, at regional scales, spreads range from 1 to 11 % (0.2 to 8.0 Tg $CH_4$ $year^{-1}$), 3 to 18 % (0.4 to 12.8 Tg $CH_4$ $year^{-1}$) and 2 to 17 % (0.1 to 12.4 Tg $CH_4$ $year^{-1}$) for re-





ACPD
15, 11853–11888, 2015

Parameterizations errors in methane inversions

R. Locatelli et al.

spectively BG, EXT and PR-LEI inversions. Across the networks, the largest spreads (in $Tg\,CH_4\,year^{-1}$) are found in China, South East Asia, Europe, South America Tropical and South America Temperate. Furthermore, spreads in surface-based inversions are larger in EXT compared to BG configuration of the surface network, similarly to what we found at the global scale. Indeed, constraints added in EXT inversions are located closer to large methane mixing ratio gradients where modelling of boundary layer mixing impact much atmospheric methane levels. Yet, skills of the different LMDz versions (LMDz-TD, LMDz-SP and LMDz-NP) to simulate PBL mixing can be highly different (Locatelli et al., 2014). Thus, the different configurations of the inverse system induce larger spreads in EXT compared to BG inversions. On average, the mean regional spread is 5, 11 and 8 % for respectively BG, EXT and PR-LEI inversions. This gives a mean error of 8 % at regional scales considering the three types of inversions.

Similarly to results found for global scale, spreads at regional scales when using different parameterizations in LMDz are smaller than spreads between inversions using different atmospheric transport models (Locatelli et al., 2013). Indeed, in Locatelli et al. (2013), spreads between inversions using different CTMs are ranged from 23 % for Europe to 48 % for South America, with an average of 33 %. Consequently, errors related to physical parameterizations explain, on average, 24 % of the total transport model errors, but it can reach more than 50 % in some specific regions. Therefore, the different parameterizations used within LMDz explore more of the transport error at regional scales than at the global scale.

Overall and across the different datasets assimilated, the parameterization producing the largest changes among the different inversions at regional scale is the thermal plume model (combined with the Yamada, 1983, scheme). It is especially true in China and in South East Asia. Among datasets, the use of satellite data compared to surface observations also induces significant changes in tropical regions (e.g. South East Asia and Tropical South America): PR-LEI-TD and PR-LEI-SP deriving larger methane emissions in South America, while PR-LEI-NP derives larger emissions in South East Asia. This uncertainty to attribute methane emissions between these two important





ACPD
15, 11853–11888, 2015

regions of the methane cycle also points towards different source categories responsible for the inferred emissions: natural wetlands for South America and anthropogenic emissions for South East Asia.

## 6 Conclusions

This study presents the sensitivity of the recent methane budget estimated by the PYVAR inversion system to different LMDz sub-grid scale physical parameterizations for vertical transport. Three versions of LMDz (LMDz-TD, LMDz-SP and LMDz-NP) have been used within the PYVAR system to simulate atmospheric transport of methane emitted at the surface. Three methane observation datasets (two surface datasets and one GOSAT satellite dataset) have been assimilated to constrain these different atmospheric inversions. Finally, the comparison between these 9 inversions quantifies the impact of LMDz sub-grid scale parameterizations on methane inverted estimates.

First, we found that surface-based and satellite-based inversions (with no bias correction) are inconsistent. It is particularly obvious when comparing surface methane measurements with methane mixing ratio simulated using methane fluxes derived by satellite-based inversion, and sampled at surface stations. We have shown here that these inconsistencies are not related to physical parameterizations of the vertical transport. We have also shown that the relative agreement between methane concentrations simulated by the former version of LMDz and GOSAT data was masking a poor representation of the methane gradient at the tropopause in the LMDz model. On the contrary, our results based on different new versions of LMDz, reproducing properly the vertical gradient of methane in the upper troposphere/lower stratosphere, suggest a bias in the GOSAT satellite data. This bias is corrected to analyse and compare the different inversions.

At the global scale, we found that the spread due to physical parameterization uncertainties is about 2.7, 7.5 and 2.1 Tg $CH_4$ year$^{-1}$ in BG, EXT and PR-LEI inversions, which represents respectively 0.5, 1.4 and 0.4 % of global methane emissions. Be-



ACPD
15, 11853–11888, 2015

sides, the analysis of the north/south gradient in inferred emissions confirms that the Emanuel (1991) deep convection scheme improves the representation of IH exchange, as it was mentioned in Locatelli et al. (2014). Indeed, inversions using Emanuel (1991) scheme (based on LMDz-SP or LMDz-NP model) have smaller interhemispheric methane emission gradients than inversions using Tiedtke, 1989, scheme (based on LMDz-TD model), which are known to simulate too fast interhemispheric exchange (Patra et al., 2011).

At regional scales, the spreads due to physical parameterization uncertainties are larger than at the global scale. The spreads in emissions over 12 continental regions represent, on average, 5.2, 10.7 and 8.2 % of the methane emissions in these regions for respectively BG, EXT and PR-LEI inversions. The thermal plume model combined with the vertical diffusion scheme of Yamada (1983) implemented in LMDz-NP largely impact regional estimations, especially when considering atmospheric constraints located close to high methane sources (like in tropical regions for satellite-based inversions).

After the quantification of transport model errors in global and regional methane flux estimates based on a TransCom intercomparison (Locatelli et al., 2013) and the evaluation of new parameterizations in LMDz to simulate trace gas concentrations (Locatelli et al., 2014), this paper goes one step further in the understanding of the causes and the impacts of model errors in methane inversions. In these different studies, we have given indications on the degree of confidence in the global and regional methane estimations using inverse modelling relatively to model errors. At the global scale, the impact of transport model errors (5 % of global methane emissions) and physical parameterizations errors (0.8 %) are acceptable. However, the picture is different at regional scales with transport errors up to 50 %, with possibly a dominant part explained by error on the vertical transport in some regions. This assessment shows that detection of methane emission anomalies at regional scales can suffer from large uncertainties due to transport errors. The emblematic example of this situation is that methane emissions in tropical regions can have an unexpected different spatio-temporal distribution





ACPD
15, 11853–11888, 2015

between continents depending on the physical parameterizations used. Such an uncertainty limits the attribution of methane emissions to particular processes, when dominant over a region. Our results push towards carrying more efforts for the improvement of transport model in order to limit transport errors by increasing collaboration between experts in atmospheric dynamics and experts in tracer transport on the one hand, and by developing measurement campaigns and specific tracers in order to better evaluate transport models on the other hand.

*Acknowledgements.* This work is supported by DGA (Direction Générale de l'Armement) and by CEA (Centre à l'Energie Atomique et aux Energies Alternatives).

We would like to thank Vanessa Sherlock, Yi Yin, Frédéric Hourdin and Catherine Rio for fruitful discussions. We would like also thank Sébastien Leonard for his IT support.

The authors wish to thank R. Parker and H. Boesch (EOS, University of Leicester) for providing the GOSAT Proxy XCH4 dataset. This product was developed partly by funding from the ESA GHG-CCI project and the UK National Centre for Earth Observation.

We acknowledge the contributors to the World Data Center for Greenhouse Gases for providing their data of methane and methyl-chloroform atmospheric mole fractions. The authors thank in particular A. J. Gomez-Pelaez (AEMET), R. Prinn (AGAGE), R. Weiss (AGAGE), P. Krummel (CSIRO), D. Worthy (EC), S. Piacentino (ENEA), Y. Fukuyama (JMA), Y. Tohjima (NIES), E. Dlugokencky (NOAA) and K. Uhse (UBA). Moreover, the authors wish to thank the respective funding organisations/institutions for their long-term support of these measurement programs.

## References

Bergamaschi, P., Krol, M., Dentener, F., Vermeulen, A., Meinhardt, F., Graul, R., Ramonet, M., Peters, W., and Dlugokencky, E. J.: Inverse modelling of national and European $CH_4$ emissions using the atmospheric zoom model TM5, Atmos. Chem. Phys., 5, 2431–2460, doi:10.5194/acp-5-2431-2005, 2005.

Bergamaschi, P., Frankenberg, C., Meirink, J. F., Krol, M., Dentener, F., Wagner, T., Platt, U., Kaplan, J. O., Körner S., Heimann, M., Dlugokencky, E. J., and Goede, A.: Satellite chartography of atmospheric methane from SCIAMACHY on board ENVISAT: 2. Eval-





ACPD

15, 11853–11888, 2015

Parameterizations errors in methane inversions

R. Locatelli et al.

Title Page
Abstract Introduction
Conclusions References
Tables Figures
◀◀ ▶▶
◀ ▶
Back Close
Full Screen / Esc
Printer-friendly Version
Interactive Discussion

uation based on inverse model simulations, J. Geophys. Res.-Atmos., 122, D02304, doi:10.1029/2006JD007268, 2007. 11858
Bergamaschi, P., Frankenberg, C., Meirink, J. F., Krol, M., Villani, M. G., Houweling, S., Dentener, F., Dlugokencky, E. J., Miller, J. B., Gatti, L. V., Engel, A., and Levin, I.: Inverse modeling of global and regional $CH_4$ emissions using SCIAMACHY satellite retrievals, J. Geophys. Res.-Atmos., 114, D22301, doi:10.1029/2009JD012287, 2009. 11866
Bergamaschi, P., Krol, M., Meirink, J. F., Dentener, F., Segers, A., van Aardenne, J., Monni, S., Vermeulen, A. T., Schmidt, M., Ramonet, M., Yver, C., Meinhardt, F., Nisbet, E. G., Fisher, R. E., O'Doherty, S., and Dlugokencky, E. J.: Inverse modeling of European $CH_4$ emissions 2001–2006, J. Geophys. Res., 115, D22309, doi:10.1029/2010JD014180, 2010.
Bergamaschi, P., Houweling, S., Segers, A., Krol, M., Frankenberg, C., Scheepmaker, R. A., Dlugokencky, E. J., Wofsy, S. C., Kort, E. A., Sweeney, C., Schuck, T., Brenninkmeijer, C., Chen, H., Beck, V., and Gerbig, C.: Atmospheric $CH_4$ in the first decade of the 21st century: Inverse modeling analysis using SCIAMACHY satellite retrievals and NOAA surface measurements, J. Geophys. Res.-Atmos., 118, 7350–7369, doi:10.1002/jgrd.50480, 2013. 11855, 11856, 11862, 11867
Bousquet, P., Hauglustaine, D. A., Peylin, P., Carouge, C., and Ciais, P.: Two decades of OH variability as inferred by an inversion of atmospheric transport and chemistry of methyl chloroform, Atmos. Chem. Phys., 5, 2635–2656, doi:10.5194/acp-5-2635-2005, 2005.
Bousquet, P., Ciais, P., Miller, J. B., Dlugokencky, E. J., Hauglustaine, D. A., Prigent, C., Van der Werf, G. R., Peylin, P., Brunke, E.-G., Carouge, C., Langenfelds, R. L., Lathiere, J., Papa, F., Ramonet, M., Schmidt, M., Steele, L. P., Tyler, S. C., and White, J.: Contribution of anthropogenic and natural sources to atmospheric methane variability, Nature, 443, 439–443, doi:10.1038/nature05132, 2006. 11858
Bousquet, P., Ringeval, B., Pison, I., Dlugokencky, E. J., Brunke, E.-G., Carouge, C., Chevallier, F., Fortems-Cheiney, A., Frankenberg, C., Hauglustaine, D. A., Krummel, P. B., Langenfelds, R. L., Ramonet, M., Schmidt, M., Steele, L. P., Szopa, S., Yver, C., Viovy, N., and Ciais, P.: Source attribution of the changes in atmospheric methane for 2006–2008, Atmos. Chem. Phys., 11, 3689–3700, doi:10.5194/acp-11-3689-2011, 2011.
Chevallier, F., Fisher, M., Peylin, P., Serrar, S., Bousquet, P., Bréon, F.-M., Chédin, A., and Ciais, P.: Inferring $CO_2$ sources and sinks from satellite observations: method and application to TOVS data, J. Geophys. Res.-Atmos., 110, D24309, doi:10.1029/2005JD006390, 2005. 11857, 11859, 11862





ACPD
15, 11853–11888, 2015

Parameterizations errors in methane inversions

R. Locatelli et al.

Chevallier, F., Bréon, F.-M., and Rayner, P. J.: Contribution of the Orbiting Carbon Observatory to the estimation of $CO_2$ sources and sinks: theoretical study in a variational data assimilation framework, J. Geophys. Res.-Atmos., 112, D09307, doi:10.1029/2006JD007375, 2007.

Chevallier, F., Feng, L., Bösch, H., Palmer, P. I., and Rayner, P. J.: On the impact of transport model errors for the estimation of $CO_2$ surface fluxes from GOSAT observations, Geophys. Res. Lett., 37, L21803, doi:10.1029/2010GL044652, 2010. 11861

Chevallier, F.: On the parallelization of atmospheric inversions of CO2 surface fluxes within a variational framework, Geosci. Model Dev., 6, 783-790, doi:10.5194/gmd-6-783-2013, 2013.

Chevallier, F., Palmer, P. I., Feng, L., Boesch, H., O'Dell, C. W., and Bousquet, P.: Toward robust and consistent regional $CO_2$ flux estimates from in-situ and spaceborne measurements of atmospheric $CO_2$, Geophys. Res. Lett., 41, 1065–1070, doi:10.1002/2013GL058772, 2014.

Cressot, C., Chevallier, F., Bousquet, P., Crevoisier, C., Dlugokencky, E. J., Fortems-Cheiney, A., Frankenberg, C., Parker, R., Pison, I., Scheepmaker, R. A., Montzka, S. A., Krummel, P. B., Steele, L. P., and Langenfelds, R. L.: On the consistency between global and regional methane emissions inferred from SCIAMACHY, TANSO-FTS, IASI and surface measurements, Atmos. Chem. Phys., 14, 577–592, doi:10.5194/acp-14-577-2014, 2014. 11858

Emanuel, K. A.: A scheme for representing cumulus convection in large-scale models, J. Atmos. Sci., 48, 2313–2329, doi:10.1175/1520-0469(1991)048<2313:ASFRCC>2.0.CO;2, 1991. 11854, 11857, 11859, 11860, 11868, 11869, 11873

Enting, I. G.: Inverse Problems in Atmospheric Constituent Transport, CUP, Cambridge, UK, 2002. 11855

Fortems-Cheiney, A., F. Chevallier, I. Pison, P. Bousquet, S. Szopa, Deeter,M. N., and Clerbaux, C.: Ten years of CO emissions as seen from Measurements of Pollution in the Troposphere (MOPITT), J. Geophys. Res.-Atmos., 116, D05304, doi:10.1029/2010JD014416, 2011.

Frankenberg, C., Meirink, J. F., van Weele, M., Platt, U., and Wagner, T.: Assessing methane emissions from global space-borne observations, Science, 308, 1010–1014, doi:10.1126/science.1106644, 2005. 11855, 11856

Frankenberg, C., Bergamaschi, P., Butz, A., Houweling, S., Meirink, J. F., Notholt, J., Petersen, A. K., Schrijver, H., Warneke, T., and Aben, I.: Tropical methane emissions: A revised view from SCIAMACHY onboard ENVISAT, Geophys. Res. Lett., 35, L15811, doi:10.1029/2008GL034300, 2008. 11856






ACPD
15, 11853–11888, 2015

Parameterizations errors in methane inversions

R. Locatelli et al.

Geels, C., Gloor, M., and Ciais, P.: Comparing atmospheric transport models for future regional inversions over Europe. Part 1: mapping the atmospheric $CO_2$ signals, Atmos. Chem. Phys., 7, 3709–3756, doi:10.5194/acp-7-3461-2007, 2007. 11856

Gilbert, J.-C., and Lemaréchal, C.: Some numerical experiments with variable-storage quasi-Newton algorithms, Math. Programm., 45, 407–435, doi:10.1007/BF01589113, 1989. 11859

Grooß, J.-U. and Russell III, James M.: Technical note: A stratospheric climatology for $O_3$, $H_2O$, $CH_4$, $NO_x$, HCl and HF derived from HALOE measurements, Atmos. Chem. Phys., 5, 2797–2807, doi:10.5194/acp-5-2797-2005, 2005. 11864

Hourdin, F. and Armengaud, A.: The use of finite-volume methods for atmospheric advection of trace species. Part I: Test of various formulations in a general circulation model, Mon. Weather Rev., 127, 822–837, doi:10.1175/1520-0493(1999)127<0822:TUOFVM>2.0.CO;2, 1999.

Hourdin, F., Couvreux, F., and Menut, L.: Parameterization of the dry convective boundary layer based on a mass flux representation of thermals, J. Atmos. Sci., 59, 1105–1123, doi:10.1175/1520-0469(2002)059<1105:POTDCB>2.0.CO;2, 2002. 11857, 11859

Hourdin, F., Musat, I., Bony, S., Braconnot, P., Codron, F., Dufresne, J.-L., Fairhead, L., Filiberti, M.-A., Friedlingstein, P., Grandpeix, J.-Y., Krinner, G., LeVan, P., Li, Z.-X., and Lott, F.: The LMDZ4 general circulation model: climate performance and sensitivity to parametrized physics with emphasis on tropical convection, Clim. Dynam., 27, 787–813, doi:10.1007/s00382-006-0158-0, 2006. 11859

Hourdin, F., Foujols, M.-A., Codron, F., Guemas, V., Dufresne, J.-L., Bony, S., Denvil, S., Guez, L., Lott, F., Ghattas, J., Braconnot, P., Marti, O., Meurdesoif, Y., and Bopp, L.: Impact of the LMDZ atmospheric grid configuration on the climate and sensitivity of the IPSL-CM5A coupled model, Clim. Dynam., 40, 2167–2192, doi:10.1007/s00382-012-1411-3, 2012a.

Hourdin, F., Grandpeix, J.-Y., Rio, C., Bony, S., Jam, A., Cheruy, F., Rochetin, N., Fairhead, L., Idelkadi, A., Musat, I., Dufresne, J.-L., Lahellec, A., Lefebvre, M.-P., and Roehrig, R.: LMDZ5B: the atmospheric component of the IPSL climate model with revisited parameterizations for clouds and convection, Clim. Dynam., 40, 2193–2222, doi:10.1007/s00382-012-1343-y, 2012b. 11859

Houweling, S., Kaminski, T., Dentener, F., Lelieveld, J., and Heimann, M.: Inverse modeling of methane sources and sinks using the adjoint of a global transport model, J. Geophys. Res., 104, 26137, doi:10.1029/1999JD900428, 1999. 11866





ACPD
15, 11853–11888, 2015

Houweling, S., Dentener, F., and Lelieveld, J.: Simulation of preindustrial atmospheric methane to constrain the global source strength of natural wetlands, J. Geophys. Res.-Atmos., 105, 17243–17255, doi:10.1029/2000JD900193, 2000.
Houweling, S., Röckmann, T., Aben, I., Keppler, F., Krol, M., Meirink, J. F., Dlugokencky, E. J., and Frankenberg, C.: Atmospheric constraints on global emissions of methane from plants, Geophys. Res. Lett., 33, L15821, doi:10.1029/2006GL026162, 2006.
Houweling, S., Aben, I., Breon, F.-M., Chevallier, F., Deutscher, N., Engelen, R., Gerbig, C., Griffith, D., Hungershoefer, K., Macatangay, R., Marshall, J., Notholt, J., Peters, W., and Serrar, S.: The importance of transport model uncertainties for the estimation of $CO_2$ sources and sinks using satellite measurements, Atmos. Chem. Phys., 10, 9981–9992, doi:10.5194/acp-10-9981-2010, 2010.
Houweling, S., Badawy, B., Baker, D. F., Basu, S., Belikov, D., Bergamaschi, P., Bousquet, P., Broquet, G., Butler, T., Canadell, J. P., Chen, J., Chevallier, F., Ciais, P., Collatz, G. J., Denning, S., Engelen, R., Enting, I. G., Fischer, M. L., Fraser, A., Gerbig, C., Gloor, M., Jacobson, A. R., Jones, D. B. A., Heimann, M., Khalil, A., Kaminski, T., Kasibhatia, P. S., Krakauer, N. Y., Krol, M., Maki, T., Maksyutov, S., Manning, A., Meesters, A., Miller, J. B., Palmer, P. I., Patra, P., Peters, W., Peylin, P., Poussi, Z., Prather, M., Randerson, J. T., Rckmann, T., Rdenbeck, C., Sarmiento, J. L., Schimel, D. S., Scholze, M., Schuh, A., Suntharalingam, P., Takahashi, T., Turnbull, J., Yurganov, L., and Vermeulen, A.: Iconic $CO_2$ time series at risk, Science (New York, NY), 337, 1038, doi:10.1126/science.337.6098.1038-b, 2012.
Houweling, S., Krol, M., Bergamaschi, P., Frankenberg, C., Dlugokencky, E. J., Morino, I., Notholt, J., Sherlock, V., Wunch, D., Beck, V., Gerbig, C., Chen, H., Kort, E. A., Röckmann, T., and Aben, I.: A multi-year methane inversion using SCIAMACHY, accounting for systematic errors using TCCON measurements, Atmos. Chem. Phys., 14, 3991–4012, doi:10.5194/acp-14-3991-2014, 2014. 11855, 11856, 11862, 11867, 11868
Kirschke, S., Bousquet, P., Ciais, P., Saunois, M., Canadell, J. G., Dlugokencky, E. J., Bergamaschi, P., Bergmann, D., Blake, D. R., Bruhwiler, L., Cameron-Smith, P., Castaldi, S., Chevallier, F., Feng, L., Fraser, A., Heimann, M., Hodson, E. L., Houweling, S., Josse, B., Fraser, P. J., Krummel, P. B., Lamarque, J.-F., Langenfelds, R. L., Le Qur, C., Naik, V., O'Doherty, S., Palmer, P. I., Pison, I., Plummer, D., Poulter, B., Prinn, R. G., Rigby, M., Ringeval, B., Santini, M., Schmidt, M., Shindell, D. T., Simpson, I. J., Spahni, R., Steele, L. P., Strode, S. A., Sudo, K., Szopa, S., van der Werf, G. R., Voulgarakis, A., van Weele, M., Weiss, R. F., Williams,





ACPD
15, 11853–11888, 2015

Parameterizations errors in methane inversions

R. Locatelli et al.

J. E., and Zeng, G.: Three decades of global methane sources and sinks, Nat. Geosci., 6, 813–823, doi:10.1038/ngeo1955, 2013. 11855

Locatelli, R., Bousquet, P., Chevallier, F., Fortems-Cheney, A., Szopa, S., Saunois, M., Agusti-Panareda, A., Bergmann, D., Bian, H., Cameron-Smith, P., Chipperfield, M. P., Gloor, E., Houweling, S., Kawa, S. R., Krol, M., Patra, P. K., Prinn, R. G., Rigby, M., Saito, R., and Wilson, C.: Impact of transport model errors on the global and regional methane emissions estimated by inverse modelling, Atmos. Chem. Phys., 13, 9917–9937, doi:10.5194/acp-13-9917-2013, 2013. 11856, 11858, 11861, 11865, 11866, 11868, 11871, 11873

Locatelli, R., Bousquet, P., Hourdin, F., Saunois, M., Cozic, A., Couvreux, F., Grandpeix, J.-Y., Lefebvre, M.-P., Rio, C., Bergamaschi, P., Chambers, S. D., Karstens, U., Kazan, V., van der Laan, S., Meijer, H. A. J., Moncrieff, J., Ramonet, M., Scheeren, H. A., Schlosser, C., Schmidt, M., Vermeulen, A., and Williams, A. G.: Atmospheric transport and chemistry of trace gases in LMDz5B: evaluation and implications for inverse modelling, Geosci. Model Dev., 8, 129–150, doi:10.5194/gmd-8-129-2015, 2015. 11856, 11860, 11863, 11866, 11867, 11870, 11871, 11873

Louis, J. F: A parametric model of vertical eddy fluxes in the atmosphere, Bound.-Lay. Meteorol., 7, 187–202, doi:10.1007/BF00117978, 1979. 11856, 11859

Monteil, G., Houweling, S., Dlugockenky, E. J., Maenhout, G., Vaughn, B. H., White, J. W. C., and Rockmann, T.: Interpreting methane variations in the past two decades using measurements of $CH_4$ mixing ratio and isotopic composition, Atmos. Chem. Phys., 11, 9141–9153, doi:10.5194/acp-11-9141-2011, 2011.

Monteil, G., Houweling, S., Butz, A., Guerlet, S., Schepers, D., Hasekamp, O., Frankenberg, C., Scheepmaker, R., Aben, I., and Röckmann, T.: Comparison of $CH_4$ inversions based on 15 months of GOSAT and SCIAMACHY observations, J. Geophys. Res.-Atmos., 118, 807–811, doi:10.1002/2013JD019760, 2013. 11855, 11866, 11867

Monteil, G. and Houweling, S.: Identifying and quantifying biases in inverse modelling of GOSAT $XCH_4$ retrievals, in preparation, 2014.

Olivier, J. G. J. and Janssens-Maenhout, G.: $CO_2$ Emissions from Fuel Combustion, IEA $CO_2$ report 2012, Greenhouse-Gas Emissions, International Energy Agency, Paris, 2012. 11858

Parker, R., Boesch, H., Cogan, A., Fraser, A., Feng, L., Palmer, P. I., Messerschmidt, J., Deutscher, N., Griffith, D. W. T., Notholt, J., Wennberg, P. O., and Wunch, D.: Methane observations from the Greenhouse Gases Observing SATellite: comparison to ground-based TCCON data and model calculations, Geophys. Res. Lett., 38, L15807, doi:10.1029/2011GL047871, 2011. 11861

Patra, P. K., Takigawa, M., Ishijima, K., Choi, B.-C., Cunnold, D., Dlugokencky, E. J., Fraser, P., Gomez-Pelaez, A. J., Goo, T.-Y., Kim, J.-S., Krummel, P., Langenfelds, R., Meinhardt, F., Mukai, H., O'Doherty, S., Prinn, R. G., Simmonds, P., Steele, P., Tohjima, Y., Tsuboi, K., Uhse, K., Weiss, R., Worthy, D., and Nakazawa, T.: Growth rate, seasonal, synoptic, diurnal variations and budget of methane in the lower atmosphere, J. Meteorol. Soc. Jpn., 87, 635–663, doi:10.2151/jmsj.87.635, 2009.

Patra, P. K., Houweling, S., Krol, M., Bousquet, P., Belikov, D., Bergmann, D., Bian, H., Cameron-Smith, P., Chipperfield, M. P., Corbin, K., Fortems-Cheiney, A., Fraser, A., Gloor, E., Hess, P., Ito, A., Kawa, S. R., Law, R. M., Loh, Z., Maksyutov, S., Meng, L., Palmer, P. I., Prinn, R. G., Rigby, M., Saito, R., and Wilson, C.: TransCom model simulations of $CH_4$ and related species: linking transport, surface flux and chemical loss with $CH_4$ variability in the troposphere and lower stratosphere, Atmos. Chem. Phys., 11, 12813–12837, doi:10.5194/acp-11-12813-2011, 2011. 11856, 11866, 11868, 11873

Patra, P. K., Krol, M. C., Montzka, S. A., Arnold, T., Atlas, E. L., Lintner, B. R., Stephens, B. B., Xiang, B., Elkins, J. W., Fraser, P. J., Ghosh, A., Hintsa, E. J., Hurst, D. F., Ishijima, K., Krummel, P. B., Miller, B. R., Miyazaki, K., Moore, F. L., Muhle, J., O'Doherty, S., Prinn, R. G., Steele, L. P., Takigawa, M., Wang, H. J., Weiss, R. F., Wofsy, S. C., and Young, D.: Observational evidence for interhemispheric hydroxyl-radical parity, Nature, 513, 219–223, doi:10.1038/nature13721, 2014.

Pison, I., Bousquet, P., Chevallier, F., Szopa, S., and Hauglustaine, D.: Multi-species inversion of $CH_4$, CO and $H_2$ emissions from surface measurements, Atmos. Chem. Phys., 9, 5281–5297, doi:10.5194/acp-9-5281-2009, 2009. 11857, 11859

Pison, I., Ringeval, B., Bousquet, P., Prigent, C., and Papa, F.: Stable atmospheric methane in the 2000s: key-role of emissions from natural wetlands, Atmos. Chem. Phys., 13, 11609–11623, doi:10.5194/acp-13-11609-2013, 2013.

Randerson, J. T., van der Werf, G. R., Giglio, L., Collatz, G. J., and Kasibhatla, P. S.: Global Fire Emissions Database, Version 3 (GFEDv3.1), available on-line [http://daac.ornl.gov/] from Oak Ridge National Laboratory Distributed Active Archive Center, Oak Ridge, Tennessee, USA, doi:10.3334/ORNLDAAC/1191, 2013. 11858





ACPD
15, 11853–11888, 2015

Parameterizations errors in methane inversions

R. Locatelli et al.

Rayner, P. and O'Brien, D.: The utility of remotely sensed $CO_2$ concentration data in surface source inversions, Geophys. Res. Lett., 28, 175–178, doi:10.1029/2000GL011912, 2001. 11866

Stephens, B. B., Gurney, K. G., Tans, P. P., Sweeney, C., Peters, W., Bruhwiler, L., Ciais, P., Ramonet, M., Bousquet, P., Nakazawa, T., Aoki, S., Machida, T., Inoue, G., Vinnichenko, N., LLoyd, J., Jordan, A., Heimann, M., Shibistova, O., Langenfelds, R. L., Steele, L. P., Francey, R. J., and Denning, A. S.: Weak northern and strong tropical land carbon uptake from vertical profiles of atmospheric $CO_2$, Science (New York, NY), 316, 1732–1735, doi:10.1126/science.1137004, 2007. 11856

Stephens, B. B., Wofsy, S. C., Keeling, R. F., Tans, P. P., and Potosnak, M. J.: The $CO_2$ Budget and Rectification Airborne Study: Strategies for Measuring Rectifiers and Regional Fluxes, Inverse Methods in Global Biogeochemical Cycles, edited by: Kasibhatla, P., Heimann, M., Rayner, P., Mahowald, N., Prinn, R. G., and Hartley, D. E., American Geophysical Union, Washington, D. C., doi:10.1029/GM114p0311, 2013.

Tiedtke, M: A comprehensive mass flux scheme for cumulus parameterization in large-scale models, Mon. Weather Rev., 117, 1779–1800, doi:10.1175/1520-0493(1989)117<1779:ACMFSF>2.0.CO;2, 1989. 11857, 11859, 11860, 11869, 11873

Yamada, T.: Simulations of nocturnal drainage flows by a Q2L turbulence closure model, J. Atmos. Sci., 40, 91–106, doi:10.1175/1520-0469(1983)040<0091:SONDFB>2.0.CO;2, 1983. 11856, 11859, 11869, 11871, 11873

Yver, C. E., Pison, I. C., Fortems-Cheiney, A., Schmidt, M., Chevallier, F., Ramonet, M., Jordan, A., Søvde, O. A., Engel, A., Fisher, R. E., Lowry, D., Nisbet, E. G., Levin, I., Hammer, S., Necki, J., Bartyzel, J., Reimann, S., Vollmer, M. K., Steinbacher, M., Aalto, T., Maione, M., Arduini, J., O'Doherty, S., Grant, A., Sturges, W. T., Forster, G. L., Lunder, C. R., Privalov, V., Paramonova, N., Werner, A., and Bousquet, P.: A new estimation of the recent tropospheric molecular hydrogen budget using atmospheric observations and variational inversion, Atmos. Chem. Phys., 11, 3375–3392, doi:10.5194/acp-11-3375-2011, 2011. 11858






ACPD
15, 11853–11888, 2015

**Table 1.** Annual hemisperic methane fluxes ($Tg\,CH_4\,year^{-1}$) for the common year of simulation (2010).

| | Northern Hemisphere (NH) | Southern Hemisphere (SH) | Difference NH – SH |
|---|---|---|---|
| PRIOR | 387.0 | 126.2 | 260.8 |
| BG-TD | 383.2 | 113.1 | 270.1 |
| BG-SP | 370.6 | 121.7 | 248.9 |
| BG-NP | 374.7 | 119.8 | 254.9 |
| EXT-TD | 386.7 | 111.4 | 275.3 |
| EXT-SP | 370.0 | 126.2 | 243.8 |
| EXT-NP | 387.1 | 117.7 | 269.4 |
| PR-LEI-TD | 376.1 | 126.2 | 249.9 |
| PR-LEI-SP | 375.4 | 126.5 | 248.9 |
| PR-LEI-NP | 382.4 | 120.3 | 262.0 |





ACPD
15, 11853–11888, 2015

**Table 2.** Spreads of regional methane flux (maximum–minimum of $CH_4$ emissions) in BG, EXT and PR-LEI inversions due to changes in physical parameterizations. The spread is expressed in percentage and in Tg $CH_4$ year$^{-1}$. The numbers are relative to the common year of inversions, which is 2010. However, average spreads between 2007 and 2011 are also showed for BG and EXT inversions (inside the brackets) since surface-based inversions have been run for several years.

| | BG | | EXT | | PR-LEI | |
|---|---|---|---|---|---|---|
| | % | Tg yr$^{-1}$ | % | Tg yr$^{-1}$ | % | Tg yr$^{-1}$ |
| North America Boreal | 5.0 (4.5) | 0.7 (0.6) | 9.4 (7.7) | 1.0 (0.9) | 2.2 | 0.3 |
| North America Temperate | 3.7 (3.4) | 1.3 (1.2) | 10.2 (9.9) | 3.8 (3.7) | 7.0 | 2.9 |
| South America Tropical | 5.6 (7.2) | 3.3 (4.0) | 10.4 (9.1) | 6.1 (5.1) | 9.8 | 6.4 |
| South America Temperate | 9.0 (8.7) | 3.1 (3.0) | 15.3 (12.5) | 5.3 (4.3) | 10.1 | 3.8 |
| Africa | 1.3 (1.2) | 0.8 (0.7) | 3.5 (2.7) | 2.1 (1.6) | 1.8 | 1.1 |
| Eurasia Boreal | 9.4 (9.4) | 1.9 (1.9) | 13.1 (14.2) | 2.6 (2.8) | 7.5 | 1.5 |
| South East Asia | 3.1 (4.0) | 2.4 (3.1) | 2.9 (3.8) | 2.3 (2.9) | 17.2 | 12.4 |
| Australia | 5.5 (6.6) | 0.2 (0.3) | 9.6 (9.8) | 0.4 (0.4) | 2.6 | 0.1 |
| Europe | 4.6 (9.0) | 1.9 (3.9) | 18.1 (13.7) | 7.4 (5.8) | 9.6 | 4.8 |
| China | 10.8 (8.6) | 8.0 (6.2) | 17.0 (10.5) | 12.8 (7.5) | 6.3 | 3.4 |
| India | 2.2 (4.8) | 0.7 (1.5) | 8.8 (6.4) | 3.1 (2.2) | 12.8 | 4.1 |
| Middle East | 2.5 (2.7) | 0.6 (0.7) | 10.0 (9.2) | 2.8 (2.4) | 9.4 | 2.7 |





ACPD
15, 11853–11888, 2015

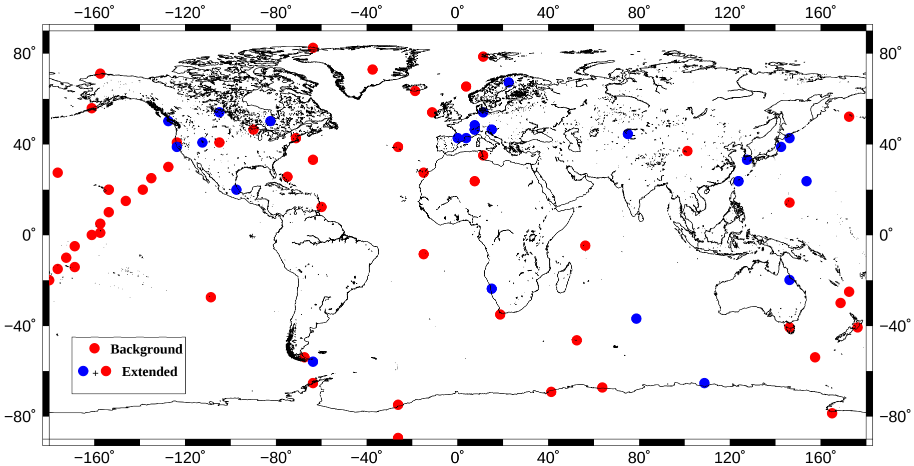


**Figure 1.** Location of the surface stations in the “background” (red circles only) and “extended” network (blue and red circles).





ACPD
15, 11853–11888, 2015

Parameterizations errors in methane inversions

R. Locatelli et al.

Title Page
Abstract Introduction
Conclusions References
Tables Figures
Back Close
Full Screen / Esc
Printer-friendly Version
Interactive Discussion

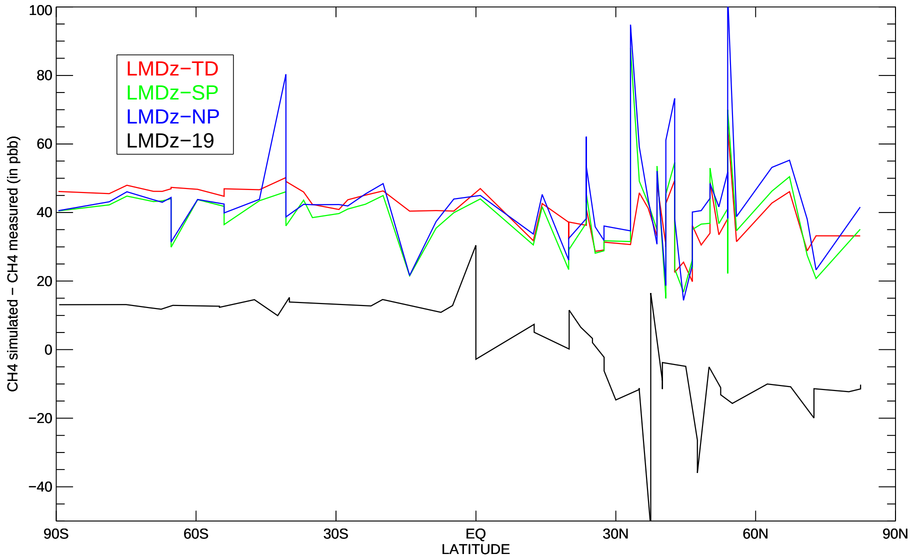


**Figure 2.** Latitudinal distribution of the bias between simulated methane mixing ratio using an optimized flux distribution coming from a satellite-based inversion and methane mixing ratio measured at different surface stations.





ACPD
15, 11853–11888, 2015

ACPD
15, 11853–11888, 2015

Parameterizations errors in methane inversions

R. Locatelli et al.





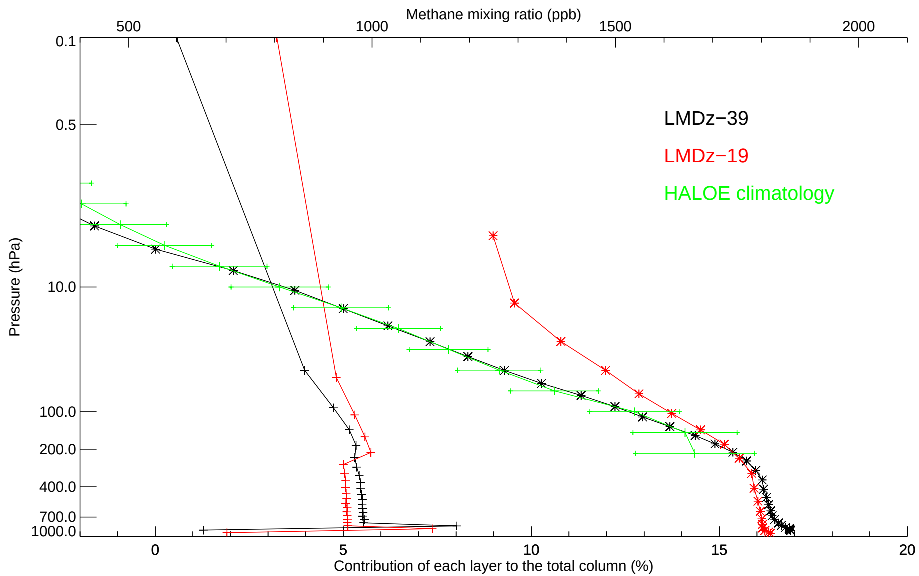


**Figure 3.** Vertical profils of methane mixing ratio in ppb (lines with stars) for LMDz-39 (red) and LMDz-19 (black) compared with HALOE climatology (green). The contribution (in percentage) of each layer of the satellite retrievals to the total column (lines with cross) is also shown for the two versions of the model.

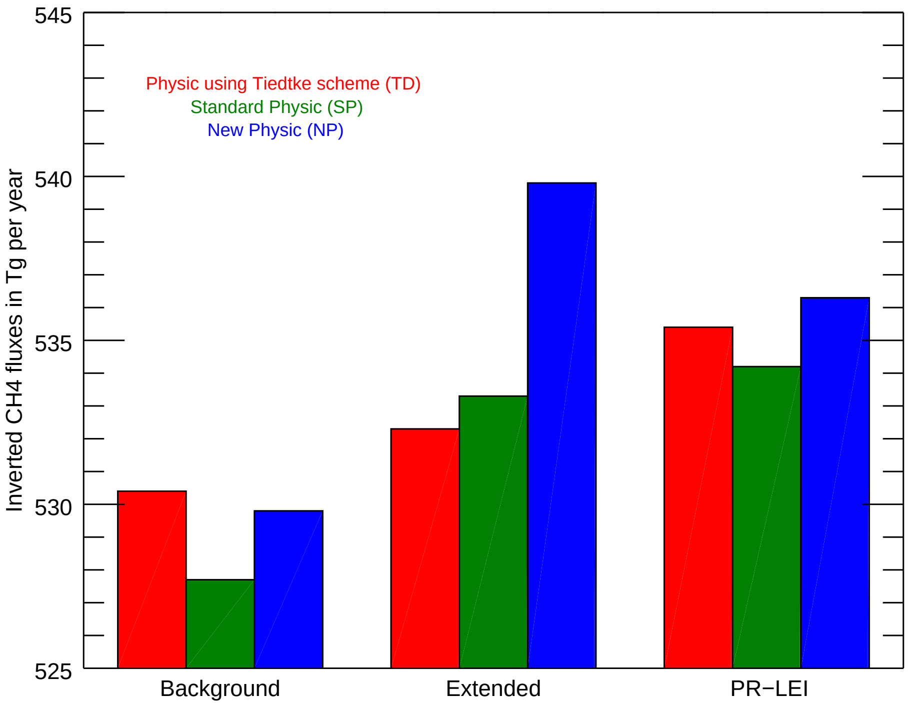


**Figure 4.** Methane flux estimates (in $Tg\,CH_4\,year^{-1}$) for 2010 at the global scale for each inversion (surface inversions using the background and the extended networks and, inversions using Proxy products provided by Leicester institude relative to GOSAT satellite). Inversions using LMDz-TD, LMDz-SP and LMDz-NP as CTM are respectively plotted in red, green and blue.





ACPD
15, 11853–11888, 2015

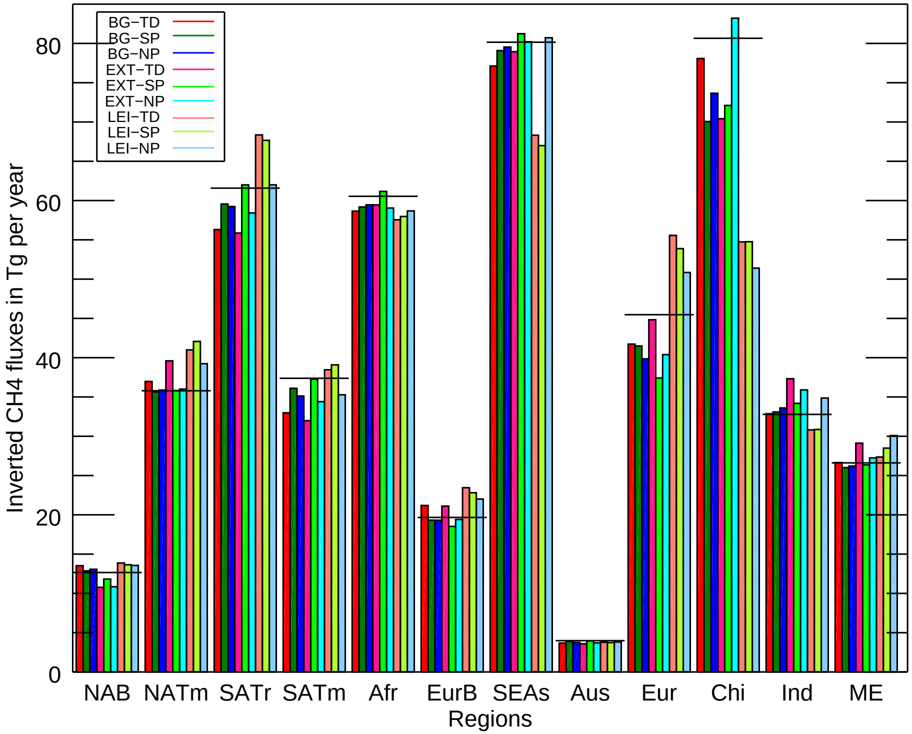


**Figure 5.** Estimations of methane fluxes for 12 regions in three versions of the model. Estimations based on LMDz-TD, LMDz-SP and LMDz-NP models are respectively represented in red, green and blue. NAB: North America Boreal; NATm: North America Temperate; SATr: South America Tropical; SATm: South America Temperate; Afr: Africa; EurB: Eurasia Boreal; SEAs: South East Asia; Aus: Australia; Eur: Europe; Chi: China; Ind: India; ME: Middle East.